A&A 375, 553–565 (2001)
DOI: 10.1051/0004-6361:20010769

Astronomy & Astrophysics

Interstellar C_2 and CN toward the Cyg OB2 association

A case study of X-ray induced chemistry

R. Gredel[1], J. H. Black[2], and M. Yan[3]

[1] Max-Planck Institut für Astronomie, Königstuhl 17, 69117 Heidelberg, Germany
e-mail: gredel@caha.es
[2] Onsala Space Observatory, Chalmers University of Technology, 43992 Onsala, Sweden
e-mail: jblack@oso.chalmers.se
[3] Harvard-Smithsonian Center for Astrophysics, 60 Garden Street, Cambridge, MA 02138, USA

Received 7 February 2001 / Accepted 23 May 2001

Abstract. An analysis of deep optical echelle spectra towards six stars in the Cyg OB2 (VI Cygni) association is presented. Interstellar absorption lines up to $J'' = 18$ in the (2,0) and (3,0) bands of the C_2 $A^1\Pi_u - X^1\Sigma_g^+$ system are detected towards Cyg OB2 No. 12. The large number of rotational lines accurately constrains the gas-kinetic temperature T and the density n to $T = 35$ K and $n = (600 \pm 100)$ cm^{-3}. The inferred C_2 column density is $N(C_2) = (20^{+4}_{-2})\,10^{13}$ cm^{-2}. The detection of various lines in the (1,0) and (2,0) band of the CN $A^2\Pi_u - X^2\Sigma^+$ red system suggest a column density of $N(CN) = (8{-}13) \times 10^{13}$ cm^{-2}. C_2 absorption lines are also detected towards Cyg OB2 No. 5 and No. 9. Inferred parameters are $T = 50$ K, $n = (600 \pm 200)$ cm^{-3}, $N(C_2) = (10^{+3.5}_{-1.5}) \times 10^{13}$ cm^{-2} towards No. 5, and $T = 100$ K, $n \geq 800$ cm^{-3}, $N(C_2) = (5.2 \pm 1) \times 10^{13}$ cm^{-2} towards No. 9. Marginal detections of C_2 towards Cyg OB2 No. 8A indicate $N(C_2) \approx 3.3 \times 10^{13}$ cm^{-2} and $T \approx 100$ K. Upper limits are $N(C_2) \leq 3.3 \times 10^{13}$ cm^{-2} toward Cyg OB2 No. 7 and No. 11. The C_2 observations eliminate the possibility that the molecular material along the line of sight towards Cyg OB2 No. 12 is spread over a pathlength of several hundred parsecs of very low density $n \approx 10$ cm^{-3}. The observations provide some support to a recent chemical model which assumes a nested structure of the molecular gas. Alternatively, the C_2 and CN abundances obtained towards Cyg OB2 No. 12 are in agreement with the predictions of an X-ray induced chemistry driven by an ionisation rate of $\zeta = (0.6{-}3) \times 10^{-15}$ s^{-1}. Calculated equilibrium temperatures of $T = 25$–50 K agree with temperatures inferred from C_2. The model also reproduces the observed column densities of CO and CH, and that of H_3^+ to within a factor of two. We predict a H_2O^+ column density of 2×10^{12} cm^{-2} towards Cyg OB2 No. 12 and H_2O^+ absorption lines which are detectable by optical absorption line techniques. We report the detection of interstellar Rubidium towards Cyg OB2 No. 12 and No. 5. Inferred column densities are $N(Rb) = (13 \pm 2) \times 10^9$ cm^{-2} towards No. 12 and $N(Rb) = (13 \pm 2) \times 10^9$ cm^{-2} towards No. 5.

Key words. ISM: abundances – ISM: clouds – ISM: molecules – X-rays: general

1. Introduction

The line of sight towards the heavily reddened star Cyg OB2 No. 12 has received renewed attention recently after the detection of very large amounts of interstellar H_3^+ (McCall et al. 1998; Geballe et al. 1999). Cyg OB2 No. 12 is classified as a B8Ia supergiant and reddened by some 10 magnitudes of visual extinction (Souza & Lutz 1980). It is generally accepted that the reddening is caused by foreground material. The star suffers from a strong stellar wind with a velocity of $V_{\rm wind} = 1400$ km s^{-1} (Leitherer et al. 1982; Bieging et al. 1989). A near-infrared excess of the star found by Leitherer et al. (1982) is attributed to free-free emission from the expanding envelope. The absence of interstellar H_2O and CO_2 ices at 3 μm and 4.27 μm, respectively, suggests that the foreground molecular material is diffuse (Whittet et al. 1997).

The H_3^+ column density towards Cyg OB2 No. 12 of $N(H_3^+) = 3.8 \times 10^{14}$ cm^{-2} is comparable to H_3^+ column densities observed in dense clouds (Geballe & Oka 1996; McCall et al. 1999). The question arises what processes are responsible for the production of such large amounts of H_3^+ in the diffuse gas, and what physical conditions prevail in the medium. In a first interpretation, McCall et al. (1998) and Geballe et al. (1999) proposed that H_3^+ forms in low density material with $n = 10$ cm^{-3} spread over pathlengths of 400–1200 pc. The authors noted, however, that their model fails to explain the abundance of CO which the authors inferred from their CO infrared observations, and that the model is in clear disagreement with earlier

Send offprint requests to: R. Gredel,
e-mail: gredel@mpia-hd.mpg.de

C_2 observations (Gredel & Münch 1994, GM94 hereafter). A detailed model of the physical and chemical structure of the line of sight towards No. 12 was recently presented by Cecchi-Pestellini & Dalgarno (2000), who proposed a nested structure of the molecular material. In their model, H_3^+ forms in diffuse gas of density $n = 50$–100 cm^{-3}, C_2 forms in embedded clouds at $n = 7000$ cm^{-3} at temperatures of $T = 35$ K, and CO forms in dense cloudlets of $n > 10^4$ cm^{-3}.

Observations of interstellar C_2 allow physical conditions such as the density and the temperature in the molecular material to be inferred. The theory of C_2 excitation was developed by van Dishoeck & Black (1982). It has been used by a variety of authors to measure densities and temperatures in diffuse and translucent molecular clouds (Gredel 1999 and references therein). Molecular carbon was detected towards No. 12 by Souza & Lutz (1977), in their discovery detection of C_2 in the interstellar medium. The authors observed the $R(2)$ and $Q(2)$ lines of the (1,0) band of the C_2 Phillips system, near 1 μm, and estimated a rotational excitation temperature of $T_{\rm ex} = 30$–40 K and a total C_2 column density of about $N(C_2) = 10^{14}$ cm^{-2}. Higher temperatures of $T_{\rm ex} = 65$ K were derived by Lutz & Crutcher (1983). A new search of C_2 towards various stars in the Cyg OB2 association resulted in the detection of the $R(2)$, $Q(2)$, and $Q(4)$ lines towards Cyg OB2 No. 12 and No. 5 by GM94. Gredel & Münch (1994) confirmed a low C_2 rotational excitation temperature towards No. 12 but failed to detect rotational lines with $J'' > 4$. Accurate column densities for levels $J'' > 4$ are required if densities are to be inferred (van Dishoeck & Black 1982).

A proper modeling of the chemistry towards Cyg OB2 No. 12 requires a knowledge of the physical conditions which prevail in the line of sight. We decided to obtain a deep optical spectrum towards No. 12, with the aim of detecting rotational lines with J$'' > 4$ so that densities may be accurately determined. The observations are described in Sect. 2. Section 3 contains a summary of the C_2 analysis and the results obtained. It includes the results of the detection of interstellar CN towards No. 12 in the (1,0) and (2,0) band of the CN $A^2\Pi_u - X^2\Sigma^+$ red system, and of interstellar Rubidium towards No. 12 and No. 5. A comparison of the derived C_2 and CN abundances with a chemical model driven by X-ray ionisation is given in Sect. 4.

2. Observations and data reduction

Interstellar absorption lines which arise from the (2,0) and (3,0) bands of the C_2 $A^1\Pi_u - X^1\Sigma_g^+$ Phillips System, around 8765 Å and 7720 Å, respectively, and of interstellar CN in the (2,0) and (1,0) bands of the CN $A^2\Pi_u - X^2\Sigma^+$ red system, around 7900 Å and 9150 Å, respectively, were searched towards stars Nos. 5, 7, 8A, 9, 11, and 12, of the Cyg OB2 association. The observations were carried out during eight nights in September 1999, using the fibre-fed echelle spectrograph FOCES of the Calar Alto Observatory 2.2 m telescope. The instrument is described in detail by Pfeiffer et al. (1998). Total integration times were two hours each for Nos. 7, 8A, 9, 11, five hours for No. 5, and twelve hours for No. 12. The 2 pixel resolution of FOCES is $R = \lambda/\Delta\lambda = 65\,000$ using a 15 μm detector. The achieved resolution is about $R = 45\,000$, as judged from the width of the thorium lines. The full optical wavelength region of 4000–10 000 Å is obtained with a single integration. The data were reduced using the MIDAS `echelle` context. The background, including the bias and the scattered light contamination, was defined by fitting a two-dimensional surface to the regions between individual orders. Pixel-to-pixel variations of the detector were corrected by use of integrations on an internal halogen lamp. The location of the spectral orders was determined using the Hough algorithm. Extracted spectra were transformed from pixel to wavelength scale using integrations on internal thorium arcs taken at the beginning and at the end of each night. The spectra were re-binned to a linear, heliocentric wavelength scale. Heliocentric velocities were inferred from the rest wavelengths of Chauville et al. (1977). Uncertainties in the velocities are estimated to be of the order of 1–1.5 km s^{-1}.

3. Analysis

3.1. Adopted molecular parameters

The measured equivalent widths W_λ of the C_2 lines were converted into column densities N using

$$N = 1.13 \times 10^{20} W_\lambda / (f_{J'J''} \lambda^2) \quad (1)$$

with W_λ and λ in units of Å and N in units of cm^{-2}. Line oscillator strengths $f_{J'J''}$ were calculated from the (2,0) band oscillator strength f_{20} from the relation $f_{J'J''} = f_{20} c S_{J'J''}/(2(2J''+1))$, with $c = \nu_{J'J''}/\nu_{\rm band}$ and Hönl-London factors $S_{J'J''}$ of $(J''+2)$, $(2J''+1)$, and $(J''-1)$ for the R, Q, and P lines, respectively. We used $f_{20} = 1.7 \times 10^{-3}$ which is obtained from an ab initio calculation by van Dishoeck (1983). The value is close to a theoretical value of $f_{20} = 1.44 \times 10^{-3}$ given by Langhoff et al. (1990), and to a measurement by Erman & Iwamae (1995) who infer $f_{20} = (1.36 \pm 0.15) \times 10^{-3}$. It is larger than $f_{20} = 1.2 \times 10^{-3}$ suggested by Lambert et al. (1995). For a recent discussion of discrepancies between theoretical and experimental f-values see Erman & Iwamae (1995) and Lambert et al. (1995). The band oscillator strength for the (3,0) band was derived from f_{20} using the theoretical ratio of $f_{20}/f_{30} = 2.2$ (van Dishoeck & Black 1982).

In the models of van Dishoeck & Black (1982) the distribution of populations of the levels J'' of C_2 is determined by the ratio $n_c\sigma_0/I$ where n_c is the density of the collision partners of C_2, $\sigma_0 = 2 \times 10^{-16}$ cm^{-2} is the cross section for collision induced transitions for level J'' to rotational level $(J''-2)$ and I is a scaling factor for the incident radiation field in the near-infrared. If a C_2 absorption oscillator strength different from the one used here is adopted, the parameter $n_c\sigma_0/I$ should be scaled by the ratio of the oscillator strengths (cf. note added in

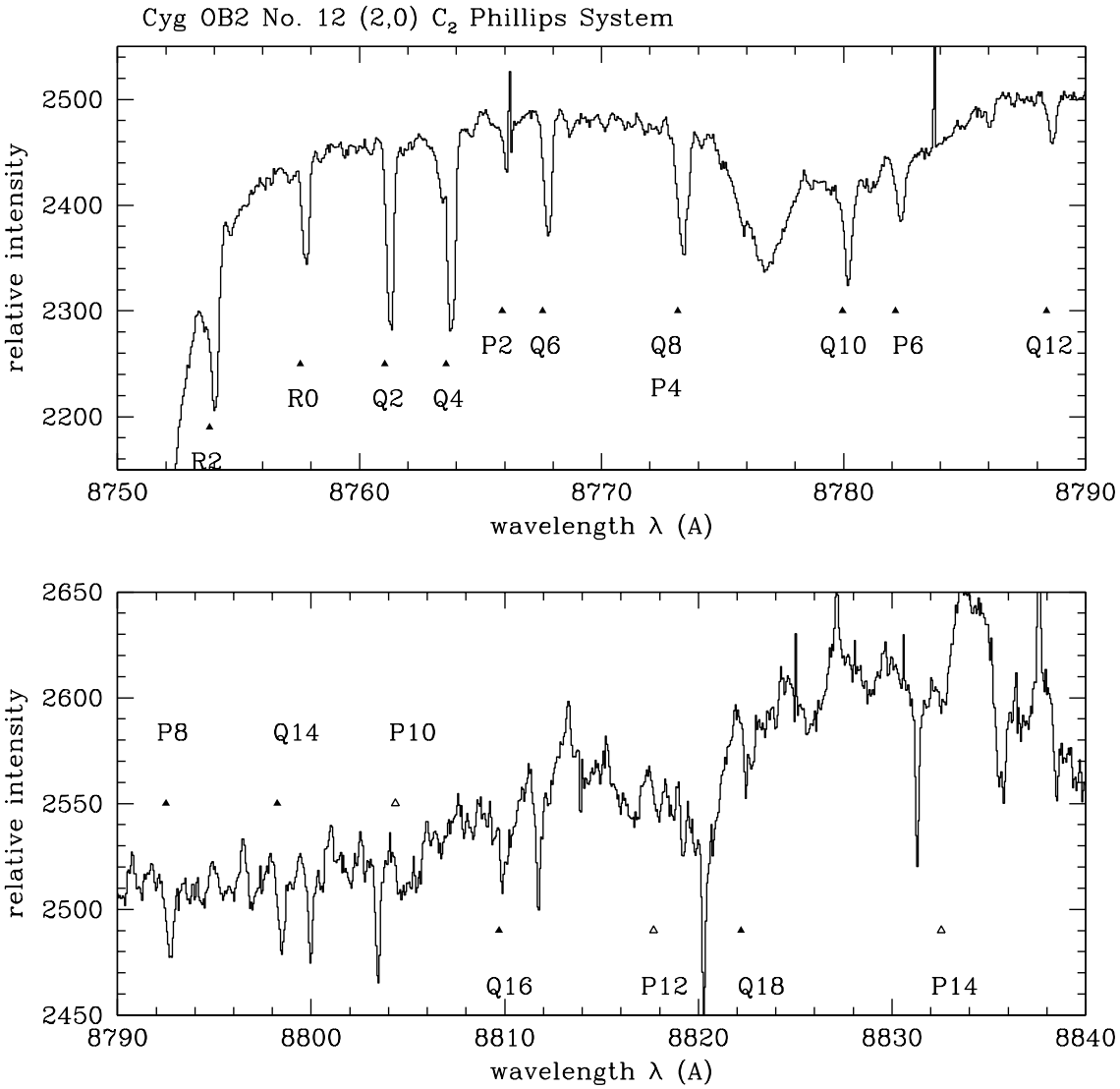

Fig. 1. Spectrum covering the (2,0) band of the C_2 Phillips System towards Cyg OB2 No. 12. Detected rotational lines are identified and marked by filled triangles. Open triangles indicate the expected positions of rotational lines which are used to infer upper limits in the populations.

proof in van Dishoeck & Black 1982). For a gas of H_2, $n_c = n(H_2)$ and $N_H = 2N(H_2)$ is the total column density of hydrogen nuclei. The density of hydrogen nuclei is $n_H = 2n_c$. We take $I = 1$ corresponding to the standard interstellar radiation field (see discussion in Sect. 4.1).

For the CN $A^2\Pi_u$ – $X^2\Sigma^+$ system, the experimental band oscillator strengths of Davis et al. (1986) of $f_{10} = 1.5 \times 10^{-3}$ and $f_{20} = 7.6 \times 10^{-4}$ were adopted for the (1,0) and (2,0) bands, respectively. Heliocentric velocities of CN were inferred from the rest wavelengths given by van Dishoeck & Black (1989).

3.2. The C_2 (2,0) and (3,0) Phillips bands

The spectrum covering the (2,0) band of the C_2 Phillips system towards Cyg OB2 No. 12 is shown in Fig. 1. The spectrum of the star is dominated by a strong stellar H I Paschen 12 line near 8752 Å and the $3p^3P - 9d^3D$ He I line near 8777 Å. Superimposed on the stellar continuum are interstellar C_2 absorption lines, which are identified. The broad absorption feature near 8763 Å is a blend of the C_2 $Q(4)$ line and of a diffuse interstellar band (cf. Sect. 3.4). The sharp absorption features near 8799.75 Å, 8803.23 Å, 8811.51 Å, 8820.05 Å, 8831.2 Å, and 8835.5 Å, arise from telluric H_2O absorption. The C_2 measurements are summarised in Table 1, where Cols. 1–5 contain the line designation, the heliocentric wavelength λ_{hel} in Å, the derived heliocentric velocity V_{hel} in km s^{-1}, the measured equivalent width W_λ in mÅ with uncertainties in parenthesis, and the derived column densities $N(J'')$ in units of 10^{13} cm^{-2}, with uncertainties in parenthesis. The colon in Col. 2 of Table 1, and in Tables 2, 3, and 6, indicates an uncertain wavelength, either because it is inferred from a line blend, or because the wavelength is indicative only in cases were upper limits in W_λ are given.

Uncertainties in W_λ are largely governed by uncertainties in the placement of the local continuum, particularly near the strong stellar H I Paschen 12 absorption line. For equivalent widths obtained from a decomposition of unresolved line blends, such as the (2,0) band $R(2) + R(10)$ blend, uncertainties are of the order of 2–3 mÅ. In general, the uncertainties are larger than 3 standard deviations of the noise in the stellar continuum. The C_2 column densities adopted here are inferred in the limit of C_2 Doppler values $b \rightarrow \infty$ (cf. Eq. (1)). A curve of growth analysis shows that deviations from the linear relation of Eq. (1) exceed values of 10% for $W_\lambda/\lambda \geq 1.7 \times 10^{-6} b$ for b in $\mathrm{km\,s^{-1}}$ for the absorption lines in the C_2 (2,0) band. Assuming a typical value of $b = 1\ \mathrm{km\,s^{-1}}$ for C_2, the C_2 lines suffer from saturation for equivalent widths of ≥15 mÅ. The strongest C_2 absorption lines have equivalent widths of $W_\lambda = 27$ mÅ. We nevertheless ignore saturation corrections for the following two reasons. Firstly, the observations of GM94 indicate the presence of two main C_2 velocity components separated by $3.7\ \mathrm{km\,s^{-1}}$. Assuming an equal distribution of the population density in both velocity components, the C_2 lines are not saturated unless $W_\lambda > 15$ mÅ per velocity component or $W_\lambda > 30$ mÅ per absorption line. Secondly, the C_2 Doppler parameter may be larger than $1\ \mathrm{km\,s^{-1}}$. The doublet ratio method applied by Chaffee & White (1982) in their analysis of K I absorption lines towards Cyg OB2 No. 12 indicates a Doppler value of $b(\mathrm{K}) = 6.4\ \mathrm{km\,s^{-1}}$ towards No. 12, with a range of $b(\mathrm{K}) = 0.7$–$10.5\ \mathrm{km\,s^{-1}}$ allowed by the measurement uncertainties. For $b(C_2) = b(\mathrm{KI})$, the C_2 lines are not saturated unless $W_\lambda > 100$ mÅ.

The spectra of stars Nos. 5, 9, 8A, 7, and 11 are shown in Fig. 2, normalised to unity and shifted by values of 0, −0.1, −0.2, −0.3, −0.4, and −0.5, respectively, along the ordinate. The scale of the ordinate applies to star No. 5. The C_2 lines detected towards Cyg OB2 No. 5 and No. 9 are summarised in Tables 2 and 3, respectively. C_2 absorption lines are marginally detected towards Cyg OB2 No. 8A. Absorption features, which may be assigned to the $Q(2)$, $Q(6)$, and $Q(8)$ lines, appear near heliocentric wavelengths of 8761.038, 8767.640, and 8773.043 Å, respectively, with equivalent widths of $W_\lambda \approx 3$ mÅ or 1–2 standard deviations. A weak diffuse interstellar band near 8763 Å is present in all five spectra.

Table 1. Summary of C_2 measurements towards Cyg OB2 No. 12.

line	λ_{hel} Å	V_{hel} km s^{-1}	W_λ mÅ	$N(J'')$ 10^{13} cm^{-2}
(3,0) band				
$R(0)$	7719.173	−6.1	7.1(2.0)	1.7(0.5)
$R(2)$	7716.407	−4.7	5.0(2.0)	3.1(1.2)
$Q(2)$	7721.997	−3.8	10.6(2.0)	5.2(1.0)
$P(2)$	7725.640[b]	−6.9	6.5(2.0)	15.9(4.9)
$Q(4)$	7724.095	−4.8	5.3(2.0)	2.6(1.0)
$Q(6)$	7727.396	−6.2	8.8(2.0)	4.3(1.0)
(2,0) band				
$R(0)$	8757.549	−4.7	14.0(1.0)	1.2(0.1)
$R(2)$	8753.810[a]	−4.8	21.1(2.0)	4.6(0.4)
$Q(2)$	8761.042	−5.2	26.9(0.5)	4.7(0.1)
$P(2)$	8765.900[b]	−4.5	5.0(2.0)	4.3(1.7)
$R(4)$	8751.493[a]	−5.6	18.9(2.0)	4.9(0.5)
$Q(4)$	8763.585[a]	−5.7	27.0(2.0)	4.7(0.3)
$P(4)$	8773.273[a]	−5.4	7.7(3.0)	4.0(1.6)
$R(6)$	8750.628	−7.5	14.7(2.0)	4.1(0.6)
$Q(6)$	8767.565	−6.6	16.6(0.5)	2.9(0.1)
$P(6)$	8782.152	−5.3	8.7(1.0)	3.9(0.4)
$Q(8)$	8773.069[a]	−5.2	14.3(3.0)	2.5(0.5)
$P(8)$	8792.495	−5.2	4.8(0.5)	2.0(0.2)
$R(10)$	8753.450[a]	−4.4	5.6(2.0)	1.7(0.6)
$Q(10)$	8779.960	−6.2	14.0(1.0)	2.4(0.2)
$P(10)$	8804.35:	...	≤3	≤1.2
$R(12)$	8756.959	−5.7	2.5(1.0)	0.8(0.3)
$Q(12)$	8788.392	−5.7	6.3(0.5)	1.1(0.1)
$P(12)$	8817.7:	...	≤1.5	≤0.6
$R(14)$	8762.0:	...	≤1.5	≤0.5
$Q(14)$	8798.265	−6.6	5.2(1.0)	0.9(0.2)
$P(14)$	8832.55:	...	≤1.5	≤0.6
$R(16)$	8768.5:	...	≤1.5	≤0.5
$Q(16)$	8809.697	−4.9	4.3(2.0)	0.7(0.3)
$R(18)$	8776.45:	...	≤1.5	≤0.5
$Q(18)$	8822.222	−7.6	3.0(1.5)	0.5(0.3)

[a] Line blend.
[b] Affected by cosmic − ray hit.

3.3. Rotational excitation of C_2

In order to obtain average column densities $<N(J'')>$ in rotational levels J'', the column densities inferred from the individual measurements in the R, P, and Q lines of the (2,0) and (3,0) bands, when available, were combined by weighting with the corresponding oscillator strengths. The gas-kinetic temperature T was determined from the rotational excitation temperature T_{ex} of the lowest rotational levels, because the population density in these levels is not significantly affected by radiative effects. Total C_2 column densities N_{tot} and densities n_{c} were obtained from theoretical fits to the population distribution, with forced agreement for $N(2)$ (cf. van Dishoeck & Black 1982). Total observed column densities were derived from the sum $N_{\mathrm{obs}} = \Sigma_{J''} N(J'')$ over the observed rotational levels.

3.3.1. Cyg OB2 No. 12

The signal to noise ratio (S/N) of the spectral region covering the (2,0) Phillips band is very high and reaches values of $S/N > 600$. Figure 3 contains an excitation diagram constructed from the detected lines, with values of $-\ln\{5N(J'')/(2J''+1)/N(2)\}$ plotted versus excitation energy $E(J'')$ of rotational level J''. Individual measurements are represented by filled triangles and upper limits by open triangles. The squares correspond to the averages $<N(J'')>$. The five lines drawn in the diagram

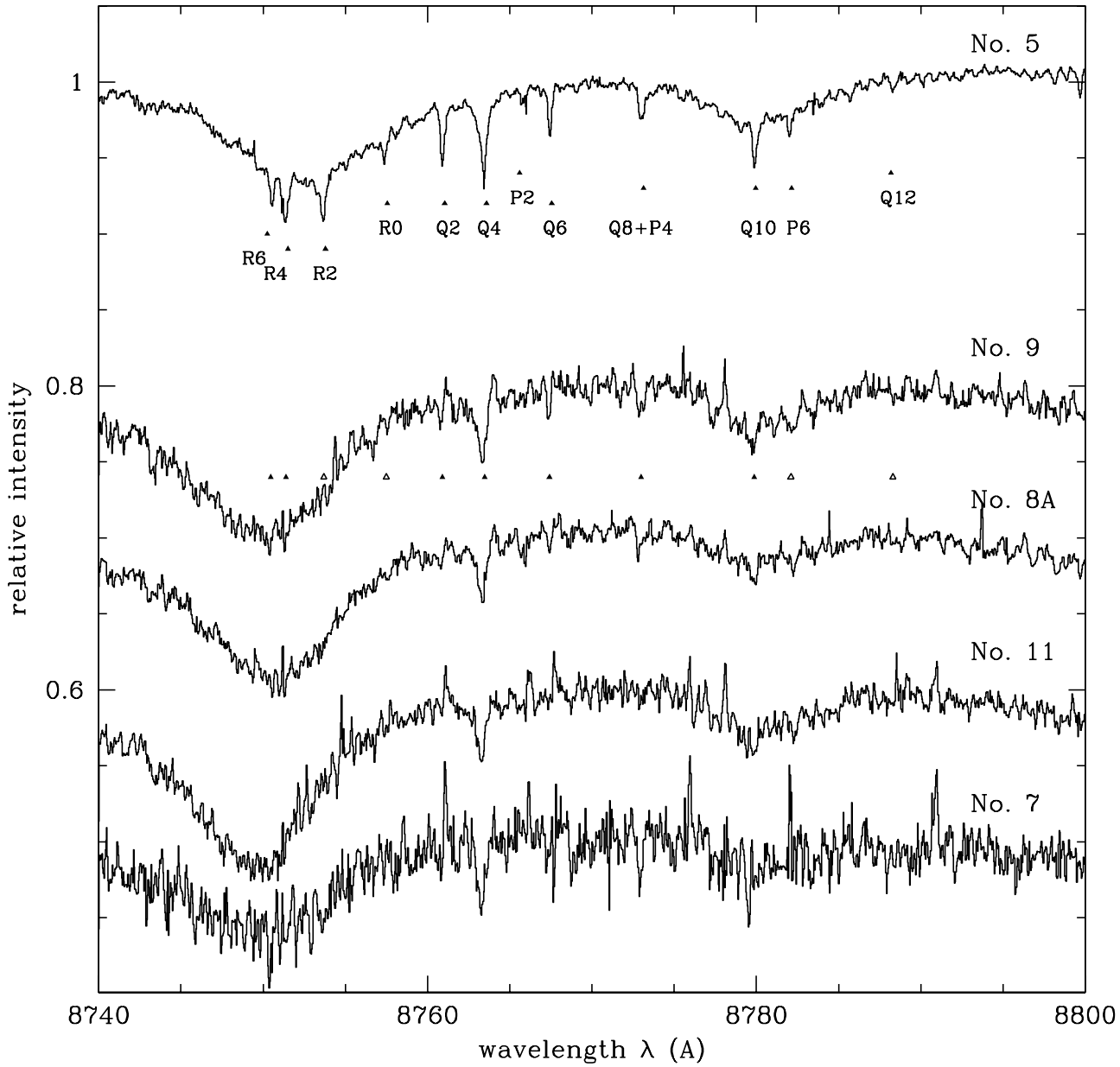

Fig. 2. Stellar spectra covering the (2,0) Phillips band towards stars Cyg OB2 Nos. 5, 9, 8A, 7, and 11. All spectra are normalised to unity and shifted along the ordinate (see text). C_2 lines detected in Cyg OB2 No. 5 are marked by filled triangles. Open triangles indicate the expected positions of rotational lines which are used to infer upper limits in the populations.

represent theoretical population distributions calculated for a temperature of $T = 35$ K and densities of collision partners of $n_c = 250$, 300, 350, 400, 450 cm^{-3}. The large number of rotational lines detected towards Cyg OB2 No. 12 sharply constrains the density n_c. The theoretical population distribution predicted for $T = 35$ K and $n_c = (300 \pm 50)$ cm^{-3} agrees with the measurements. The total density of hydrogen is $n = (600 \pm 100)$ cm^{-3}. The theoretical total C_2 column density derived from $N(2)$ and T and n_c is $N_{tot} = (20^{+4}_{-2}) \times 10^{13}$ cm^{-2}. The total observed column density is $N_{obs} = 21 \times 10^{13}$ cm^{-2}. The average C_2 velocity, derived by weighting individual velocities with the absorption oscillator strengths of the corresponding absorption lines, is V_{hel} (C_2) $= -5.5$ km s^{-1}.

3.3.2. Cyg OB2 Nos. 5, 7, 8A, 9, 11

The excitation diagrams constructed for Cyg OB2 No. 5 and No. 9 are shown in Figs. 4 and 5. The observed population distribution towards No. 5 is reproduced well by $T = 50$ K and $n_c = 300 \pm 100$ cm^{-3}. The parameters indicate a total C_2 column density $N_{tot} = (10.3^{+3.5}_{-1.5}) \times 10^{13}$ cm^{-2}. The total observed column density is $N_{obs} = 10.3 \times 10^{13}$ cm^{-2}. The average heliocentric velocity is V_{hel} (C_2) $= -7.9$ km s^{-1}.

The excitation diagram constructed for No. 9 is less constraining than that for No. 12 or No. 5. The population density in the $J'' = 0-8$ rotational levels may be described by a thermal population distribution at $T = 100$ K.

Table 2. Cyg OB2 No. 5, C_2 (2,0) Phillips band.

line	$\lambda_{\rm hel}$ Å	$V_{\rm hel}$ km s^{-1}	W_λ mÅ	$N(J'')$ 10^{13} cm^{-2}
$R(0)$	8757.383	−10.4	5.5(3.0)	0.5(0.3)
$R(2)$	8753.698[a]	−8.6	10.5(1.5)	2.3(0.3)
$Q(2)$	8760.962	−7.9	11.0(1.5)	1.9(0.3)
$P(2)$	8765.770	−8.9	3.0(2.0)	2.6(1.7)
$R(4)$	8751.404[a]	−8.7	10.5(1.5)	2.7(0.4)
$Q(4)$	8763.482	−9.2	10.0(2.5)	1.7(0.4)
$P(4)$	8773.1:[a]	...	3.5(3.0)	1.8(1.6)
$R(6)$	8750.573	−9.4	7.0(3.0)	2.0(0.8)
$Q(6)$	8767.470	−9.9	8.3(1.5)	1.4(0.3)
$P(6)$	8782.060	−8.5	4.5(2.0)	2.0(0.9)
$R(8)$	8751.31[a]	−6.1	3.5(2.0)	1.0(0.6)
$Q(8)$	8773.1:[a]	...	6.5(3.0)	1.1(0.5)
$R(10)$	8753.345[a]	−8.0	3.5(1.5)	1.1(0.5)
$Q(10)$	8779.938	−6.9	8.5(2.0)	1.5(0.3)
$R(12)$	8756.9:	...	≤1.5	≤0.5
$Q(12)$	8788.350	−7.1	3.0(2.0)	0.5(0.3)
$R(14)$	8761.9:	...	≤1.5	≤0.5
$Q(14)$	8798.270	−6.4	3.0(2.0)	0.5(0.3)
$R(16)$	8768.2:	...	≤1.5	≤0.5
$Q(16)$	8809.570	−9.2	3.0(2.0)	0.5(0.3)

[a]Line blend.

Table 3. Cyg OB2 No. 9, C_2 (2,0) Phillips band.

line	$\lambda_{\rm hel}$ Å	$V_{\rm hel}$ km s^{-1}	W_λ mÅ	$N(J'')$ 10^{13} cm^{-2}
$R(0)$	8757.5:	...	≤3	≤0.3
$R(2)$	8753.7:	...	≤3	≤0.7
$Q(2)$	8760.906	−9.9	3.8(2)	0.7(0.3)
$R(4)$	8751.381	−9.5	4.5(2)	1.2(0.5)
$Q(4)$	8763.485[a]	−9.1	9.0(2)	1.6(0.3)
$P(4)$	8773.16:[a]	...	2.4(2)	1.2(1)
$R(6)$	8750.455	−13.4	2.5(2)	0.7(0.6)
$Q(6)$	8767.409	−12.0	4.8(2)	0.8(0.3)
$P(6)$	8782.1:	...	≤3	≤1.3
$Q(8)$	8772.92:[a]	...	3.4(2)	0.6(0.3)
$P(8)$	8792.365	−9.7	2.5(2)	1.0(0.8)
$Q(10)$	8779.871	−9.2	4.0(2)	0.7(0.3)
$Q(12)$	8788.3:	...	≤3	≤0.5

[a]Line blend.

The fit to the population densities in $J'' = 0-8$ yields $N(2) = 0.95 \times 10^{13}$ cm^{-2} which is adopted in the following as $N(2)$. The population density in $J'' = 10$ and the upper limit in $J'' = 12$ suggest $n_{\rm c} > 400$ cm^{-3}. For $T = 100$ K, $n_{\rm c} > 400$ cm^{-3}, and $N(2)$, the modeled total C_2 column density is $N_{\rm tot} = (5.2 \pm 1) \times 10^{13}$ cm^{-2}. The observations yield $N(C_2) = 5.1 \times 10^{13}$ cm^{-2}. The average heliocentric velocity is $V_{\rm hel}$ (C_2) = −10.2 km s^{-1}.

The marginal detections of a few Q-branch lines towards Cyg OB2 No. 8A yield column densities of about $N(J'') \approx 0.5 \times 10^{13}$ cm^{-2} in each of $J'' = 2$, 6, and 8. The total observed column density is $N_{\rm obs} \approx 1.5 \times 10^{13}$ cm^{-2}.

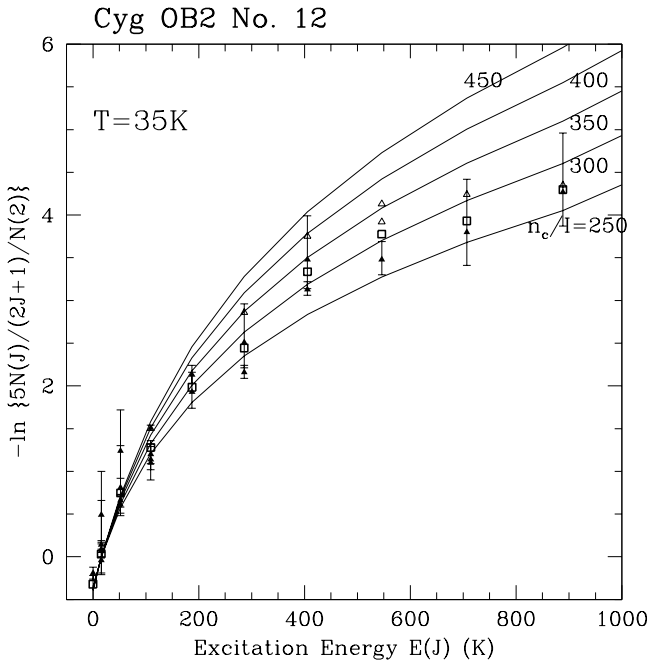

Fig. 3. C_2 excitation diagram of Cyg OB2 No. 12, with rotational population densities plotted versus excitation energies $E(J'')$. Filled triangles correspond to individual line detections, open triangles are upper limits. Open squares are averages for individual rotational levels. The five lines drawn in the diagram represent theoretical population distributions obtained at gas-kinetic temperatures of $T = 35$ K and densities of collision partners of $n_{\rm c}/I = 250$, 300, 350, 400, 450 cm^{-3}.

The population distribution in rotational levels $J'' = 2$, 6, and 8 indicates a rotational excitation temperature of $T_{\rm ex} = 100$ K. Assuming the kinetic temperature $T = 100$ K and a thermal distribution, we obtain a value of $N_{\rm tot} = 3.3 \times 10^{13}$ cm^{-2}. The mean heliocentric velocity of the three absorption lines is $V_{\rm hel}$ (C_2) = −5.2 km s^{-1}. Towards Cyg OB2 No. 7 and Cyg OB2 No. 11, the upper limits on the $Q(2)$ line correspond to $N(2) < 0.5 \times 10^{13}$ cm^{-2}, or $N_{\rm tot} \le 3.3 \times 10^{13}$ cm^{-2} towards both stars, for a thermal population distribution at $T = 100$ K. The C_2 column density is $N_{\rm tot} \le 2.5 \times 10^{13}$ if T were less than 50 K.

3.3.3. Comparison with previous results

Our C_2 measurements are consistent with previous results. The first detection of C_2 towards Cyg OB2 No. 12 (Souza & Lutz 1977) yielded a column density in the $J'' = 2$ level of $N(2) = 4.6 \times 10^{13}$ cm^{-2}, rescaled to the absorption oscillator strength adopted here. Our value is 4.85×10^{13} cm^{-2}. The column densities of GM94, in units of 10^{13} cm^{-2}, are $N(0) = 1.1$, $N(2) = 5.1$, and $N(4) = 4.2$, respectively, again rescaled to the absorption oscillator strength of van Dishoeck (1983). Our values are $N(0) = 1.4$, $N(2) = 4.85$, $N(4) = 4.3$. Towards No. 5, GM94 measured $N(0) = 0.5$, $N(2) = 2.4$, and $N(4) = 1.6$, all in units of 10^{13} cm^{-2}, which compares with our data

Table 4. Summary of C_2 measurements in Cyg OB2.

star, spectral type	A_V mag	T K	n_c cm^{-3}	$N(2)$ 10^{13} cm^{-2}	N_{tot} 10^{13} cm^{-2}	N_{obs} 10^{13} cm^{-2}	V_{hel} $km\,s^{-1}$
No. 12, B8Ia	10.1	35	300 ± 50	4.85	20^{+4}_{-2}	21.0	−5.5
No. 5, O7Ia	6.0	50	300 ± 100	2.1	$10^{+3.5}_{-1.5}$	10.3	−7.9
No. 9, O5If	6.7	100	≥400	0.95	5.2 ± 1	5.1	−10.2
No. 8a, O6Ib	4.8	[100]	...	1.5	3.3	1.5	[−5.2]
No. 7, O3If	5.3	...	...	≤0.5	<3.3	...	...
No. 11, O5If	5.3	...	...	≤0.5	<3.3	...	...

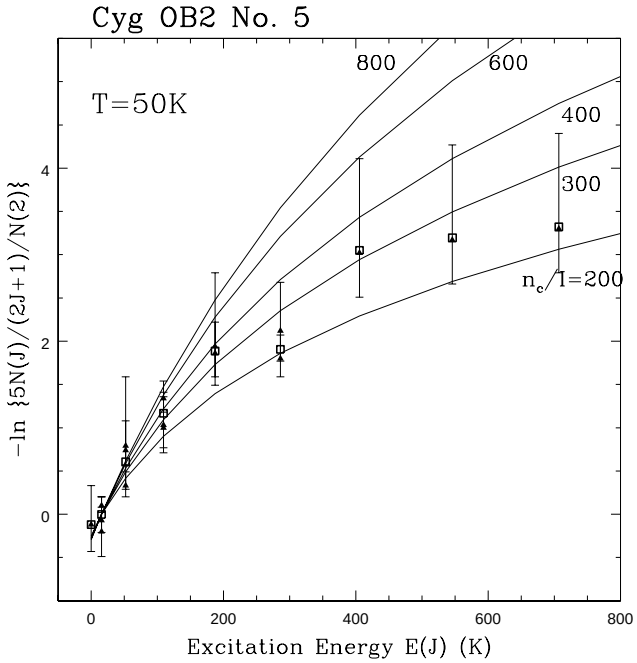

Fig. 4. Rotational excitation diagram for Cyg OB2 No. 5. Symbols as in Fig. 3. The five lines correspond to theoretical population distributions obtained at $T = 50$ K and densities of $n_c/I = 200$, 300, 400, 600, 800 cm^{-3}.

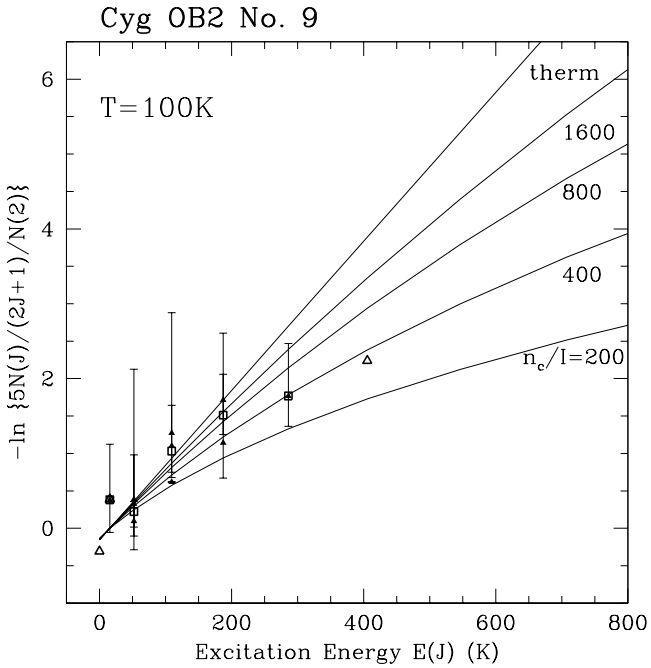

Fig. 5. Rotational excitation diagram for Cyg OB2 No. 9. Symbols as in Fig. 3. The five lines correspond to densities of $n_c/I = 200$, 400, 800, 1600 cm^{-3}, and a thermal distribution at $T = 100$ K.

of $N(0) = 0.5$, $N(2) = 2.1$, and $N(4) = 2.1$. In general, our measured equivalent widths are consistent with those of Lutz & Crutcher (1983). Exceptions occur for the $P(4)+Q(8)$ line blend, where Lutz & Crutcher (1983) obtain 22 ± 3 mÅ, compared to our value of 30.5 ± 3 mÅ, and the $R(0)$ line, where Lutz & Crutcher (1983) give 19.1 ± 3.2 mÅ, compared to our value of 14 ± 1 mÅ.

The observations of GM94 were taken at the higher spectral resolution of $R = 65\,000$ and indicate a total of four absorption components towards No. 12, two unresolved components at $V_{hel} = -5.7$ and -2.5 $km\,s^{-1}$, and two weaker components near -10.6 $km\,s^{-1}$ and $+13.6$ $km\,s^{-1}$. This agrees reasonably well with our detection of a single, unresolved absorption line near $V_{hel} = -5.5$ $km\,s^{-1}$. The absorption components near -10.6 $km\,s^{-1}$ and $+13.6$ $km\,s^{-1}$ of GM94 are not present in our spectrum, which has a significantly higher S/N compared to the spectra of GM94. They may thus not be real.

Table 4 summarises the C_2 measurements towards the Cyg OB2 association. It contains, in Cols. 1–8, respectively, the star and its spectral type, its visual extinction A_V as given by Humphreys (1978), the gas-kinetic temperature T, the density n_c, the column density in rotational level $J'' = 2$, the total C_2 column density N_{tot} inferred from T, n_c and $N(2)$, the total observed column density N_{obs}, and the average heliocentric velocity V_{hel}. In the discussion of Sect. 4, theoretical C_2 column densities N_{tot} are used in the comparison with chemical models, rather than N_{obs}, because the theoretical column densities include the population densities in the unobserved levels as well.

3.4. Diffuse interstellar bands near 7721 Å and 8763 Å

The spectra of all six stars in Cyg OB2 observed here are affected by absorption bands near 7721 Å and near 8763 Å which are broader than the interstellar C_2 lines. These bands were previously identified as new diffuse interstellar

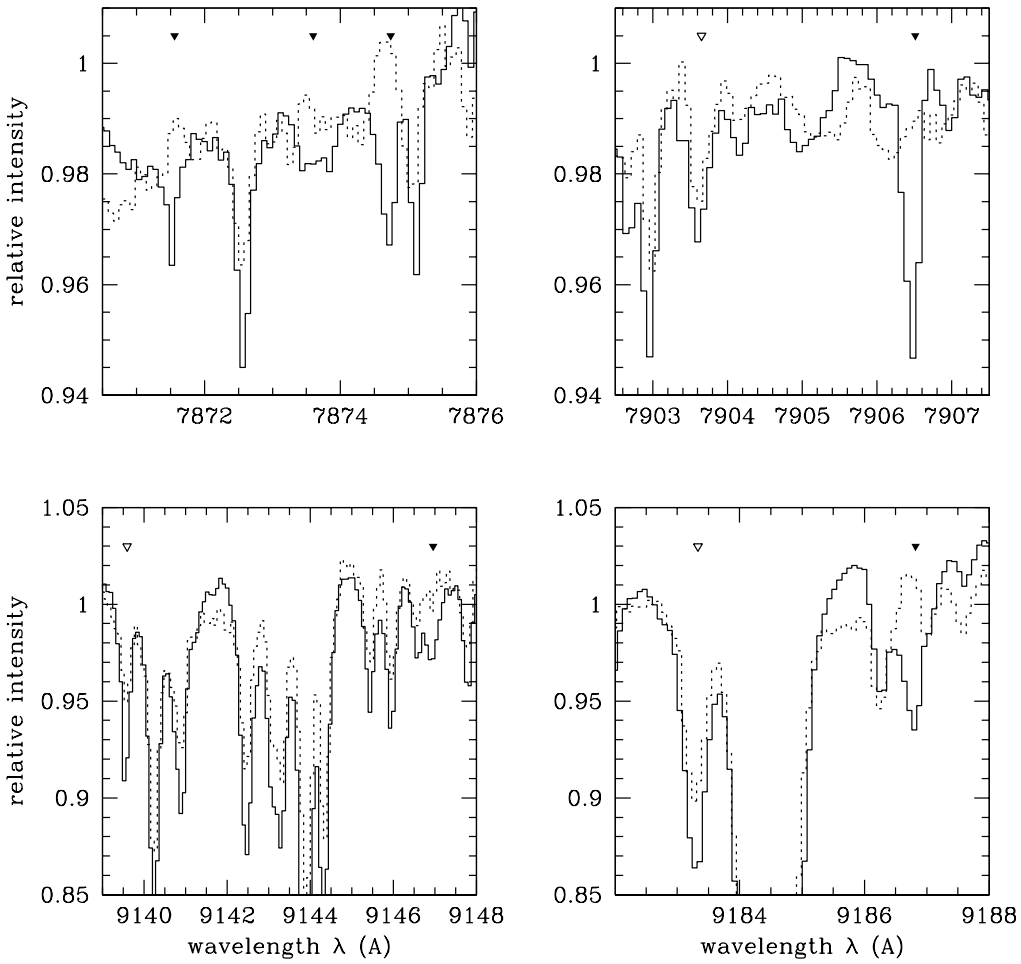

Fig. 6. Normalised spectra covering the (2,0) band and (1,0) bands of the CN $A^2\Pi_u$ – $X^2\Sigma^+$ red system towards Cyg OB2 No. 12 (bold lines). Comparison spectra of η Tau are represented by dotted lines. The locations of various CN lines (cf. Table 6) are given by triangles.

bands (DIBs) (Herbig & Leka 1991; Gredel & Münch 1986). A complete discussion of the DIBs will be presented elsewhere. Table 4 summarises the measurements of the band near 8763 Å, with the star, the wavelength, the full width at half maximum (*FWHM*), and the equivalent width of the band, listed in Cols. 1–4, respectively. It has been suggested that DIBs form largely in low-density, diffuse material (Herbig 1995). We note here that the DIB towards Cyg OB2 No. 12 is relatively weak compared with the other stars in Cyg OB2. Such is not expected if the line of sight towards No. 12 passes through a high column density of low density material spread over a pathlength of some 1000 pc (cf. discussion in Sect. 4.1).

Table 5. The 8763 Å diffuse interstellar band towards Cyg OB2.

star	$\lambda_{\rm hel}$ Å	*FWHM* Å	W_λ mÅ
No. 12	8763.43	0.61	12
No. 5	8763.59	0.61	25
No. 9	8763.45	0.61	16
No. 8A	8763.52	0.51	18
No. 7	8763.48	0.56	24
No. 11	8763.47	0.60	13

3.5. The CN (2,0) and (1,0) $A^2\Pi_u - X^2\Sigma^+$ red system

The spectral region which covers the absorption lines of the (1,0) and (2,0) bands of the CN red system is heavily contaminated by telluric absorption lines. However, a few lines in the (1,0) and (2,0) bands are well isolated and accurate equivalent widths can be determined.

Figure 6 contains the normalised spectra towards Cyg OB2 No. 12. The position of the detected CN lines is indicated by filled triangles. Open triangles mark the expected positions of CN absorption lines which are blended with atmospheric features. The (2,0) ${}^SR_{21}(0)$ (7871.5 Å), (2,0) $[{}^RQ_{21}(1) + R_2(1)]$ (7873.9 Å), (2,0) ${}^RQ_{21}(0)$ (7874.7 Å), (2,0) $R_1(0)$ (7906.5 Å), (1,0) $[{}^QP_{21}(1) + Q_2(1)]$ (9146.9 Å), and (1,0) $R_1(0)$ (9186.8 Å) lines or line blends, are clearly detected. The measurements

allow the determination the column density $N(0)$ in the rotational level $N'' = 0$. The lack of clear detections of absorption lines arising from the rotational level $N'' = 1$ constrains the column density $N(1)$. In order to judge what the maximum CN abundance is towards Cyg OB2 No. 12, upper limits are estimated for the (2,0) $R_1(1)$ (7903.6 Å), (1,0) ${}^SR_{21}(0)$ (9139.6 Å), and (1,0) $R_1(1)$ (9183.3 Å) lines. The estimate was obtained from a comparison of the relative strengths of the telluric lines in Cyg OB2 No. 12 and in η Tau. The spectrum of η Tau is represented in Fig. 6 by the dotted line. CN is not detected towards η Tau. Upper limits estimated for the column density in $N'' = 1$ agree reasonably well with the column density inferred from the marginally detected (1,0)$[{}^QP_{21}(1)+Q_2(1)]$ line blend near 9147 Å.

The CN measurements are summarised in Table 6. It gives, in Cols. 1–6, the line designation, the measured heliocentric wavelength $\lambda_{\rm hel}$ and the heliocentric velocity $V_{\rm hel}$, the measured equivalent width W_λ, and the inferred column densities $N(0)$ and $N(1)$ in the $N'' = 0$ and $N'' = 1$ rotational levels, respectively. Uncertainties are given in parentheses. The last row contains in Cols. 5 and 6, respectively, the average column density $N(0)$ inferred from the observations and the column density $N(1)$ in the limit where the CN excitation temperature T_{10} is close to the cosmic microwave background radiation temperature of 2.7 K. The row above contains the value $N(1)$ estimated from the observations, and the corresponding CN excitation temperature in Col. 7. A firm lower limit to the total CN column density towards Cyg OB2 No. 12 is $N({\rm CN}) > 8 \times 10^{13}$ cm^{-2}, and the upper limit is $N({\rm CN}) < 13 \times 10^{13}$ cm^{-2}. The average heliocentric velocity of CN is -4.3 km s^{-1} which is consistent with the velocity of C_2.

3.6. Interstellar Rubidium towards Cyg OB2 No. 12 and No. 5

We report the detection of the interstellar Rb I $5s^2S_{1/2} - 5p^2P_{3/2}$ resonance line near 7800 Å towards Cyg OB2 No. 12 and towards No. 5. This presents the first firm detection of rubidium in the interstellar medium. The significance of an earlier Rb I measurement by Jura & Smith (1981) towards ζ Oph has been questioned by Federman et al. (1985), who did not detect Rb I in their high quality spectra towards ζ Oph and towards two other lines of sight.

Our spectra are shown in Fig. 7. The Rb I line is detected at 10 standard deviations towards Cyg OB2 No. 12. We use the formalism and the atomic data of Morton (2000) to transfer measured equivalent widths of (5 ± 0.5) mÅ and (2.7 ± 0.5) mÅ towards No. 12 and No. 5, respectively, into column densities of $N({\rm Rb\ I}) = (13 \pm 2) \times 10^9$ cm^{-2} and $N({\rm Rb\ I}) = (7 \pm 2) \times 10^9$ cm^{-2}. Heliocentric velocities are $V_{\rm hel} = -6.4$ km s^{-1} for No. 12 and -8.1 km s^{-1} towards No. 5, respectively. The Rb I velocities agree with those of C_2 within the errors.

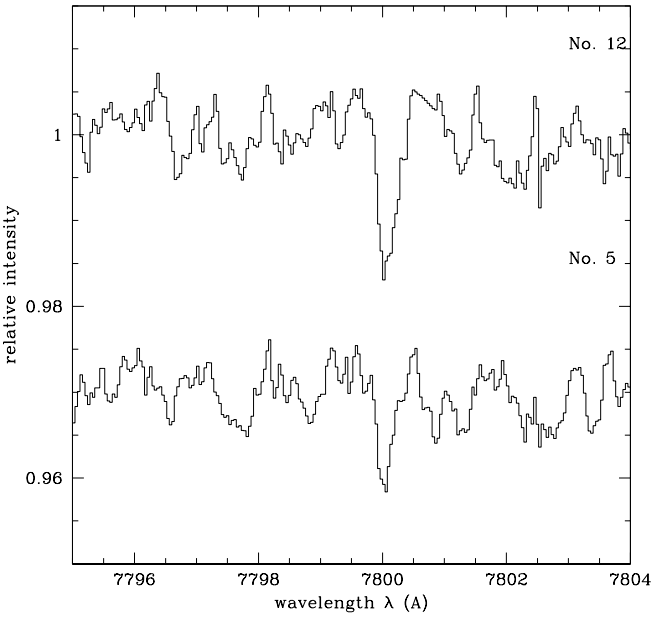

Fig. 7. Detection of the interstellar line of Rb I $5s^2S_{1/2} - 5p^2P_{3/2}$ towards Cyg OB2 No. 12 and No. 5. The spectrum of No. 5 is shifted by 0.03 units along the ordinate.

Neutral rubidium has an ionisation potential of 4.77 eV, thus interstellar rubidium is mostly ionised. The ionisation potential is similar to that of potassium, and relative abundances of $N({\rm Rb^+})/N({\rm K^+})$ may be related to measured ratios $N({\rm Rb})/N({\rm K})$ (Federman et al. 1985). Column densities of $N({\rm K}) = 3.3 \times 10^{12}$ cm^{-2} towards No. 12 and $N({\rm K}) = 2.2 \times 10^{12}$ cm^{-2} towards No. 5 were inferred by Chaffee & White (1982). The K I 7664 Å and 7698 Å absorption lines are also present in our spectra. The K I 7698 Å line is well separated from a telluric O_2 absorption line but the K I 7664 Å line is not. Equivalent widths of the K I 7698 Å lines are 382 ± 10 mÅ and 275 ± 10 mÅ, respectively, towards No. 12 and No. 5. The measured equivalent widths are consistent with those inferred by Chaffee & White (1982), who give 323 ± 59 towards No. 12 and 294 ± 48 towards No. 5. Using the atomic parameters of Morton (1991), we infer $N({\rm K}) = 2 \times 10^{12}$ cm^{-2} towards No. 12 and $N({\rm K}) = 1.5 \times 10^{12}$ cm^{-2} towards No. 5. These values, calculated in the limit of unsaturated lines, are close to the neutral K column densities derived Chaffee & White (1982) who used the doublet ratio to estimate saturation corrections.

The K I column densities inferred by Chaffee & White (1982) and the Rb I column densities inferred here suggest values of $N({\rm Rb^+})/N({\rm K^+}) = (0.8{-}1) \times 10^{-3}$ towards Cyg OB2. This ratio compares with upper limits of $N({\rm Rb^+})/N({\rm K^+}) \leq 1.5 \times 10^{-3}$ inferred by Federman et al. (1985) towards *o* Per, ζ Per, and ζ Oph. The ${\rm Rb^+/K^+}$ ratio towards No. 12 is about a factor of three lower than the solar ratio of $N({\rm Rb^+})/N({\rm K^+}) = 2.9 \times 10^{-3}$ (as given in Federman et al. 1985).

Table 6. Summary of CN absorption lines towards Cyg OB2 No. 12.

transition	$\lambda_{\rm hel}$ Å	$V_{\rm hel}$ km s^{-1}	W_λ mÅ	$N(0)$ 10^{12} cm^{-2}	$N(1)$ 10^{12} cm^{-2}	T_{10} K
$(2,0)^S R_{21}(0)$	7871.562	−3.1	3.5(2)	61(35)		
$(2,0)[^R Q_{21}(1) + R_2(1)]$	7873.873	−4.4	4.5(2)		50(22)	
$(2,0)^R Q_{21}(0)$	7874.742	−4.0	10(5)	72(36)		
$(2,0)R_1(1)$	7903.65:	...	≤6		≤64	
$(2,0)R_1(0)$	7906.507	−3.6	10(2)	45(9)		
$(1,0)^S R_{21}(0)$	9139.6:	...	≤28	≤180		
$(1,0)[^Q P_{21}(1) + Q_2(1)]$	9146.960	−7.9	14.3(5)		77(27)	
$(1,0)R_1(1)$	9183.3:	...	≤53		≤210	
$(1,0)R_1(0)$	9186.817	−3.8	25(5)	42(8)		
				56	70	6.2
				56	23	2.7

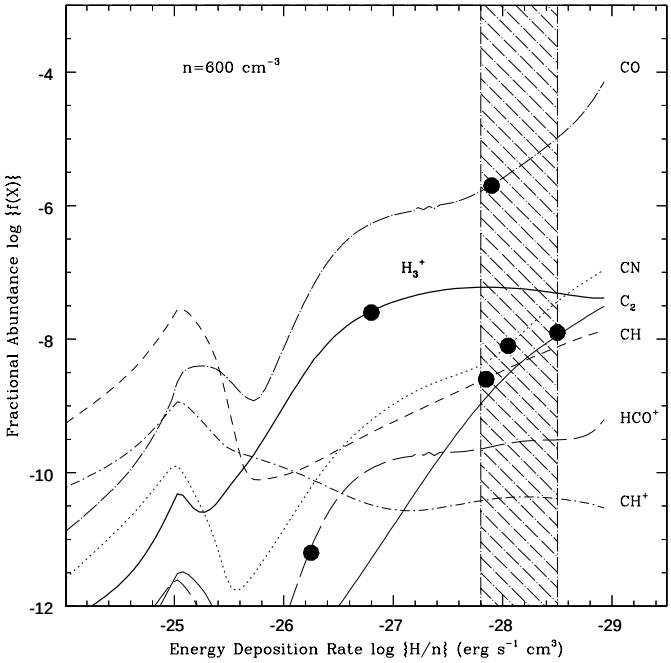

Fig. 8. Fractional molecular abundances f(X) plotted versus X-ray energy deposition rate H/n calculated for a model of $n = 600$ cm^{-3} and N(H) $= 1.6 \times 10^{22}$ cm^{-2}. Dots are fractional molecular abundances towards Cyg OB2 No. 12 inferred from observations. The shaded region corresponds to X-ray ionisation rates of $\zeta = (0.6{-}3) \times 10^{-15}$ s^{-1}.

4. Discussion

The absence of circumstellar material around No. 12 was inferred from direct near-infrared photometry of the star, carried out using a multi-filter Ge bolometer (Persi & Ferrari-Toniolo 1982; Leitherer et al. 1982). No. 12 has been identified, however, as the optical counterpart of an IRAS source (Parthasarathy et al. 1992). Parthasarathy et al. (1992) interpreted their mid-infrared IRAS observations to indicate the presence of warm ($T = 900$ K) and cold dust ($T = 80$ K) around the star. From an analysis of the wavelength dependence of the polarisation, McMillan & Tapia (1977) concluded that the reddening arises in two uniformly polarising slabs, one of them possibly located within the Cyg OB2 association. Massey & Thompson (1991) have suggested that the high luminosity of the star coupled with its high extinction is in fact not a coincidence, but may provide evidence of a previous episode of mass loss, and that the large visual extinction of the star is mainly circumstellar. If so, the detection of unusual isotope ratios may provide an observational test. We have searched our spectra for the presence of ^{12}C^{13}C absorption lines. We use mass-scaled rotational constants and the molecular parameters of Amiot & Verges (1983) to obtain wavelengths of ^{12}C^{13}C. The R-branch bandhead of the (2,0) band of the ^{12}C^{13}C Phillips system is located near 8792 Å, and the $Q(1)$–$Q(10)$ lines of the (2,0) band are located in the 8808–8830 Å region. Our spectrum shown in Fig. 1 does not contain absorption features which may be associated with ^{12}C^{13}C. Upper limits are $W_\lambda < 0.5$ mÅ. The vibrational transition probabilities of ^{12}C^{13}C are similar than those of C_2 (Halmann & Laulicht 1966). ^{12}C^{13}C is a hetero-nuclear molecule and all rotational levels in the various electronic states are present. Consequently, the ^{12}C^{13}C population density is spread over twice as many rotational levels as for C_2. The ratio of the equivalent widths of the say $Q(2)$ absorption lines from C_2 and ^{12}C^{13}C is >54. This value leads to an estimate of $N(C_2)/N(^{12}C^{13}C) > 27$. Assuming that $N(C_2)/N(^{12}C^{13}C) = a^2/2a$ where a is the ^{12}C/^{13}C isotope ratio, we obtain a value of $a > 54$ towards Cyg OB2 No. 12, which is consistent with the interstellar value of $a = 65$ and which agrees within a factor of two with the terrestrial value of $a = 89$. This finding provides little evidence that the extinction towards No. 12 is largely circumstellar.

4.1. C_2 and CN formation in quiescent translucent clouds

Observed molecular column densities towards No. 12 are $N(H_3^+) = 3.8 \times 10^{14}$ cm^{-2} and N(CO) $= 2.6 \times 10^{16}$ cm^{-2} (McCall et al. 1998; Geballe et al. 1999),

$N(C_2) = 2 \times 10^{14}$ cm^{-2} and $N(CN) = (0.8-1.3) \times 10^{14}$ cm^{-2} (present work), $N(CH) = 4.1 \times 10^{13}$ cm^{-2}, and $N(HCO^+) = 10^{11}$ cm^{-2} (Scappini et al. 2000). The CH column density is inferred from an emission line near $V_{hel} = -4.7$ km s^{-1} (Willson 1984). Note that McCall et al. (1998) do not include saturation corrections when inferring CO column densities. The CO column density may be significantly larger than cited. The presence of strong interstellar absorption lines from CH and CH^+ was reported by Souza & Lutz (1980), but neither equivalent widths nor molecular column densities are given. Because of the large reddening of Cyg OB2 No. 12, the signal to noise ratio in the blue wavelength region of our spectrum is very low, and neither the CH^+ (4232 Å) nor the CH (4300 Å) absorption lines are detected.

The visual extinction of $A_V = 10$ mag towards No. 12 corresponds to a total hydrogen column density of $N(H) = 1.6 \times 10^{22}$ cm^{-2}. The observed molecular column densities are converted to fractional abundances $f(X) = N(X) / N(H)$ of $f(H_3^+) = 2.4 \times 10^{-8}$, $f(C_2) = 1.25 \times 10^{-8}$, $f(CN) = (5-8) \times 10^{-9}$, $f(CO) = 1.6 \times 10^{-6}$, $f(CH) = 2.6 \times 10^{-9}$, and $f(HCO^+) = 6.25 \times 10^{-12}$.

The models of McCall et al. (1998) and Geballe et al. (1999) reproduce the observed column density of H_3^+ by assuming that the molecular material along the line of sight towards Cyg OB2 is dominated by diffuse material of average density $n = 10$ cm^{-3} spread over pathlengths of some 400–1200 parsec. The authors note that the model does not produce the observed abundances of C_2 and CO. The presence of clumps of molecular gas with densities of $n_c = (300 \pm 50)$ cm^{-3}, or $n = (600 \pm 100)$ cm^{-3}, towards Cyg OB2 No. 12, is demonstrated from the C_2 observations presented above.

A model by Cecchi-Pestellini & Dalgarno (2000) avoids the assumption of long pathlength and produces the observed abundance of H_3^+ from a nested structure for the clouds. In their model, H_3^+ is formed in low density clouds of $n = 50$–100 cm^{-3}, C_2 is formed in embedded cloudlets at temperatures $T = 35$ K and $n = 7 \times 10^3$ cm^{-3}, and CO is formed in high density cores of $n = 10^5$ cm^{-3} or greater. The model also predicts a HCO^+ column density of $N(HCO^+) = 9 \times 10^9$ cm^{-2}. The recent detection of HCO^+ towards No. 12 by Scappini et al. (2000) provides further and strong support to a model with dense cores embedded in lower density material.

The gas-kinetic temperature of the C_2-containing cloudlets inferred from the present observations agree very well with the prediction of the model of Cecchi-Pestellini & Dalgarno (2000). The densities inferred from C_2 are significantly lower though, unless a value of $I = 11$ is adopted as the scaling factor of the radiation field of the general background starlight. We have modeled the radiation field from the 44 most luminous stars in the association (cf. Sect. 4.2). We find that the molecular gas will have to be closer than 100 pc to the association in order for it to dominate the radiation field, which we consider unlikely. We conclude that the C_2 observations do indicate a low gas density, rather than a grossly enhanced radiation field.

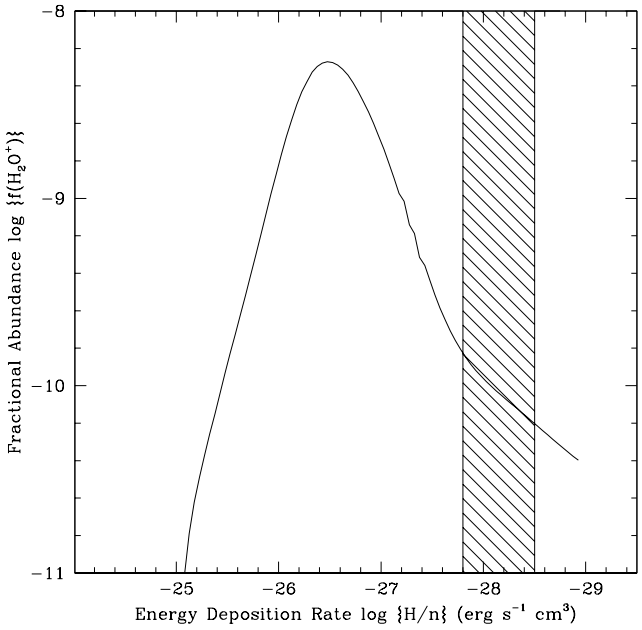

Fig. 9. Fractional abundances of H_2O^+ plotted versus X-ray energy deposition rate H/n calculated for a model of $n = 600$ cm^{-3} and $N(H) = 1.6 \times 10^{22}$ cm^{-2}. The shaded region corresponds to ionisation rates of $\zeta = (0.6-3) \times 10^{-15}$ s^{-1}.

4.2. X-ray induced chemistry towards Cyg OB2

The stars Cyg OB2 Nos. 5, 8A, 9, and 12, are all very powerful X-ray emitters (Kitamoto & Mukai 1996; Waldron et al. 1998). If molecular gas is exposed to X-rays, its chemistry will be modified by increased photoionisation rates caused by X-ray absorptions. In order to estimate whether X-rays may affect the chemical composition of the translucent cloud towards Cyg OB2, we have modeled the radiation field of the 44 most luminous stars with $M_V < -4$ mag of Massey & Thompson (1991). We obtain a total luminosity of 7×10^{50} s^{-1} ionising photons and a total of 3×10^{45} s^{-1} of X-ray photons. Note that these are lower limits as the Cygnus OB2 region may contain up to 2600 OB stars (Knödlseder 2000). We use the radio observations of Downes & Rinehart (1966) to estimate an emission measure of $EM = 6450$ cm^{-6} pc and an electron density of $n_e = 34$ cm^{-3} towards No. 12. The large number of ionising photons will support a Strömgren sphere of 104 pc at an electron density of $n_e = 34$ cm^{-3}. This is roughly the size of the 5 GHz free-free emission region seen in the radio map of Downes & Rinehart (1966). The stellar winds may have evacuated such a large region already that the nebula is density-bounded, and thus leaking photons into the neighboring neutral gas. We conclude that an X-ray driven chemistry may very well provide an alternative scenario for the formation of molecules towards the Cygnus OB2 region.

The effects of X-rays on the chemistry of translucent molecular clouds have been modeled by Lepp & Dalgarno (1996). They presented steady-state abundances of various interstellar molecules as a function of ζ/n, where ζ is the X-ray ionisation rate in units of s^{-1}.

The observed fractional abundances of CO, CH, HCO^+, and CN, are all well reproduced for ionisation rates per density of $\zeta/n = (1-3) \times 10^{-17}$ s^{-1} cm^3, or $\zeta = (1-2) \times 10^{-15}$ s^{-1} for densities of $n = 600$ cm^{-3}. The fractional abundance of CH and CN is also reproduced with the lower ionisation rate of $\zeta = 6 \times 10^{-18}$ s^{-1}, but that of the other molecules is not. The lower ionisation rate is close to the cosmic ray ionisation rate of dark clouds.

Maloney et al. (1996) showed that the physics and the chemistry of an X-ray irradiated gas are predominantly determined by the local X-ray energy deposition rate per particle H divided by the particle density n. Comprehensive models of the energy deposition of X-rays in atomic and molecular gas and the effects of the X-rays on the chemistry were developed by Yan (1996), who calculated fractional molecular abundances as a function of H/n. A full discussion of the models and the chemical network used will be presented elsewhere. The parameter H, expressed in units of erg s^{-1} per hydrogen nucleus, is related to the X-ray ionisation rate ζ in units of s^{-1} per hydrogen molecule by $\zeta = 3 \times 10^{10} H$ (Yan 1996). Here we use the models of Yan (1996) to calculate the fractional abundances of H_3^+, CO, C_2, CN, CH, and HCO^+. In all simulations, the total hydrogen density is fixed to a value of $N_{\rm H} = 1.6 \times 10^{22}$ cm^{-2} and the density is $n = 600$ cm^{-3}. Figure 8 contains the calculated fractional molecular abundances as a function of H/n. Filled dots are fractional abundances inferred from the observations. The shaded region corresponds to values of $\zeta = (0.6-3) \times 10^{-15}$ s^{-1}. The observed fractional abundances of CO, C_2, CN, and CH, are well reproduced for this range of X-ray ionisation rates. The inferred ionisation rates agree with those suggested by the models of Lepp & Dalgarno (1996). The modeled fractional H_3^+ abundance is $f(H_3^+) = 5 \times 10^{-8}$, which corresponds to a column density of $N(H_3^+) = 8 \times 10^{14}$ cm^{-2}. Thus, our model falls short by a factor of two to reproduce the H_3^+ column density towards Cyg OB2 No. 12.

The models of Yan (1996) determine the gas temperature and the grain temperature by solving the heating and cooling balance equations. The equilibrium temperatures which result for ionisation rates of $\zeta = (0.6-3) \times 10^{-15}$ s^{-1} are 25–50 K, which agree perfectly with the gas-kinetic temperature derived from the C_2 observations.

We derive large abundances of H_2O^+ in our model. Figure 9 contains a plot of the fractional H_2O^+ abundance as a function of H/n. At the ionisation rates inferred above, again represented by the shaded region, $f(H_2O^+)$ is of the order of 10^{-10}. H_2O^+ peaks with $f(H_2O^+) = 6 \times 10^{-9}$ at high ionisation rates of $\zeta \approx 6 \times 10^{-14}$ s^{-1}. We predict that towards Cyg OB2 No. 12, H_2O^+ absorption lines which arise from the $\tilde{A}^2A_1 - \tilde{X}^2B_1$ system are detectable in the optical wavelength region. We use the molecular parameters of Lew (1976) to calculate the air wavelengths given in Table 7. Oscillator strengths are from Lutz (1987). Towards Cyg OB2 No. 12, the predicted H_2O^+ fractional abundance corresponds to a column density of $N(H_2O^+) = 2 \times 10^{12}$ cm^{-2}. The strongest lines, such as the 1_{10}–0_{00} transition of the $(0,4,0)-(0,0,0)$ band near 8057.7 Å (cf. Table 7), will have equivalent widths of some $W_\lambda \approx 0.5$ mÅ. The H_2O^+ absorption lines are strong enough to be detectable by optical absorption line techniques. Our spectrum towards Cyg OB2 No. 12 covers all H_2O^+ lines given in Table 7, but it is not of sufficient quality to unequivocally identify H_2O^+. At the resolution adopted here, H_2O^+ will be detectable in spectra with $S/N > 1000$.

Table 7. Predicted air wavelengths of H_2O^+.

band	transition	$\bar{\nu}$ cm^{-1}	$\lambda_{\rm air}$ λ	f
(0,4,0) − (0,0,0)	$1_{10}-0_{00}$	12407.079	8057.698	4.0×10^{-4}
		12423.239	8047.217	
	$2_{11}-1_{01}$	12424.403	8046.463	2.0×10^{-4}
		12434.249	8040.091	
	$1_{11}-1_{01}$	12385.413	8071.794	2.0×10^{-4}
		12401.999	8060.999	
(0,6,0) − (0,0,0)	$1_{10}-0_{00}$	14335.600	6973.717	4.5×10^{-4}
		14342.930	6970.153	
	$2_{11}-1_{01}$	14352.573	6965.470	2.25×10^{-4}
		14356.980	6963.332	
	$1_{11}-1_{01}$	14313.203	6984.629	2.25×10^{-4}
		14320.860	6980.895	

5. Conclusions

We have presented observations of interstellar absorption lines of C_2 and CN towards Cyg OB2 No. 12. The C_2 observations indicate low densities of $n = 600 \pm 100$ cm^{-3} of the molecular gas. We find evidence that the chemistry of the translucent cloud towards Cyg OB2 is affected by X-rays. We reproduce the observed column densities of C_2, CN, CH, and CO, for X-ray ionisation rates of $\zeta = (0.6-3) \times 10^{-15}$ s^{-1}. The observed column density of H_3^+ is reproduced to within a factor of two. We predict large amounts of H_2O^+ towards Cyg OB2 No. 12 which will be detectable by optical absorption line techniques.

Acknowledgements. It is a pleasure to thank Alex Dalgarno for most fruitful discussions and suggestions. The careful reading of the manuscript by the referee, Dr. S. R. Federman, is kindly acknowledged.

References

Amiot, C., & Verges, J. 1983, A&AS, 51, 257
Chauville, J., Maillard, J. P., & Mantz, A. W. 1977, J. Molec. Spectr., 68, 399
Bieging, J. H., Abbott, D. C., & Churchwell, E. B. 1989, ApJ, 340, 518
Cecchi-Pestellini, C., & Dalgarno, A. 2000, MNRAS, 313, L6
Chaffee, F. H., Jr., & White, R. E. 1982, ApJS, 50, 169
Davis, S. P., Shortenhaus, D., Stark, G., et al. 1986, ApJ, 303, 892
Downes, D., & Rinehart, R. 1966, ApJ, 144, 937
van Dishoeck, E. F. 1983, Chem. Phys., 77, 277

van Dishoeck, E. F., & Black, J. H. 1982, ApJ, 258, 533
van Dishoeck, E. F., & Black, J. H. 1989, ApJ, 340, 273
Erman, P., & Iwamae, A. 1995, ApJ, 450, L31
Federman, S. R., Sneden, C., Schrempp, W. V., & Smith, W. H. 1985, ApJ, 290, L55
Geballe, T. R., & Oka, T. 1996, Nature, 384, 334
Geballe, T. R., McCall, B. J., Hinkle, K. H., & Oka, T. 1999, ApJ, 510, 251
Gredel, R. 1999, A&A, 351, 657
Gredel, R., & Münch, G. 1986, A&A, 154, 336
Gredel, R., & Münch, G. 1994, A&A, 285, 640 (GM94)
Halmann, M., & Laulicht, I. 1966, ApJS, 110, 307
Herbig, G. H. 1995, ARA&A, 33, 19
Herbig, G. H., & Leka, K. D. 1991, ApJ, 382, 193
Humphreys, R. M. 1978, ApJS, 38, 309
Jura, M., & Smith, W. H. 1981, ApJ, 251, L43
Knödlseder, J. 2000, A&A, 360, 539
Kitamoto, S., & Mukai, K. 1996, PASJ, 48, 813
Lambert, D. L., Sheffer, Y., & Federman, S. R. 1995, ApJ, 438, 740
Langhoff, S. R., Bauschlicher, C. W., Jr., Rendell, A. P., & Komornicki, A. 1990, J. Chem. Phys., 92, 300
Leitherer, C., Hefele, H., Stahl, O., & Wolf, B. 1982, A&A, 108, 102
Lepp, S., & Dalgarno, A. 1996, A&A, 306, L21
Lew, H. 1976, Canad. J. Phys., 54, 2028
Lutz, B. L. 1987, ApJ, 315, L147
Lutz, B. L., & Crutcher, R. M. 1983, ApJ, 271, L101
Maloney, P. R., Hollenbach, D. J., & Tielens, A. G. G. M. 1996, ApJ, 466, 561
Massey, P., & Thompson, A. B. 1991, AJ, 101, 1408
McCall, B. J., Geballe, T. R., Hinkle, K. H., & Oka, T. 1999, ApJ, 522, 338
McCall, B. J., Geballe, T. R., Hinkle, K. H., & Oka, T. 1998, Science, 279, 1910
McMillan, R. S., & Tapia, S. 1977, ApJ, 212, 714
Morton, D. C. 1991, ApJS, 77, 119
Morton, D. C. 2000, ApJS, 130, 403
Parthasarathy, M., Jain, S. K., & Bhatt, H. C. 1992, A&A, 266, 202
Persi, P., & Ferrari-Toniolo, M. 1982, A&A, 111, L7
Pfeiffer, M. J., Frank, C., Baumüller, D., Fuhrmann, K., & Gehren, T. 1998, A&AS, 130, 381
Scappini, F., Cecchi-Pestellini, C., Codella, C., & Dalgarno, A. 2000, MNRAS, 317, L6
Souza, S. P., & Lutz, B. L. 1977, ApJ, 216, L49
Souza, S. P., & Lutz, B. L. 1980, ApJ, 235, L87
Waldron, W. L., Corcoran, M. F., Drake, S. A., & Smale, A. P. 1998, ApJS, 118, 217
Whittet, D. C. B., Boogert, A. C. A., Gerakines, P. A., et al. 1997, ApJ, 490, 729
Yan, M. 1996, The Influence of X-rays on Molecular Clouds, Ph.D. Thesis, Harvard University, Cambridge, Massachusetts, December 1996